


FULL PAPER

Atomistic hybrid particle-field molecular dynamics combined with slip-springs: Restoring entangled dynamics to simulations of polymer melts

Zhenghao Wu¹  | Andreas Kalogirou¹ | Antonio De Nicola² | Giuseppe Milano² | Florian Müller-Plathe¹

¹Eduard-Zintl-Institut für Anorganische und Physikalische Chemie, Technische Universität Darmstadt, Darmstadt, Germany

²Department of Organic Materials Science, Yamagata University, Yamagata-ken, Japan

Correspondence

Florian Müller-Plathe, Eduard-Zintl-Institut für Anorganische und Physikalische Chemie, Technische Universität Darmstadt, Alarich-Weiss-Str. 8, 64287 Darmstadt, Germany.
Email: f.mueller-plathe@theo.chemie.tu-darmstadt.de

Funding information

Deutsche Forschungsgemeinschaft, Grant/Award Number: SFB-TRR 146

Abstract

In hybrid particle-field (hPF) simulations (*J. Chem. Phys.*, **2009** 130, 214106), the entangled dynamics of polymer melts is lost due to chain crossability. Chains cross, because the field-treatment of the *nonbonded* interactions makes them effectively soft-core. We introduce a multi-chain slip-spring model (*J. Chem. Phys.*, **2013** 138, 104907) into the hPF scheme to mimic the topological constraints of entanglements. The structure of the polymer chains is consistent with that of regular molecular dynamics simulations and is not affected by the introduction of slip-springs. Although slight deviations are seen at short times, dynamical properties such as mean-square displacements and reorientational relaxation times are in good agreement with traditional molecular dynamics simulations and theoretical predictions at long times.

KEYWORDS

atomistic, dynamics, entangled polymer, hybrid particle-field simulation, slip-spring

1 | INTRODUCTION

Atomistic molecular dynamics (MD) calculations provide, in principle, all the information desired for soft-matter systems: structure, thermodynamics, and dynamics. In many practical applications, however, they are too computationally expensive to allow the treatment of large enough systems for long enough times. This has led to numerous efforts to derive coarse-grained (CG) models, which are simplified by aggregating a varying number of atoms into single superatoms. The different coarse-graining procedures ensure that the CG models still reproduce some aspects of the studied systems.^[1] In this contribution, we follow a different route to make MD calculations faster. First, we maintain the description of the *bonded* interactions at the desired

level, which can be itself by CG or, as in this paper, atomistic. Second, the *nonbonded* interactions are approximated by the interactions of atoms with a potential field, which is, in turn, determined from the atomic density. This so-called hybrid particle-field molecular dynamics (hPF-MD) method was introduced by Milano and Kawakatsu a decade ago.^[2] It borrows several implementation tricks from the self-consistent-field (SCF) theory.^[3,4]

In hPF-MD, the nonbonded forces acting on a particle are expressed as function of the derivatives of local density gradients. This reformulation enables much more efficient simulations than standard MD as the evaluation of *nonbonded* pair forces is replaced by building particle-to-mesh density fields and computing the density field potentials. Both steps are of first order in the number of particles. The hPF-MD model has been demonstrated to be effective to investigate homopolymers and block copolymers at both CG^[2] and atomistic resolutions.^[5,6] More recently, the hPF-MD model was

[Correction added on 09 September 2020, after first online publication: Projekt Deal funding statement has been added.]

validated in describing the conformational and dynamical properties of biological systems such as lipid bilayers^[7-9] and bio-surfactants.^[10,11] After the integration of electrostatics,^[12,13] the hPF-MD method was further successfully applied in charged systems particularly of polyelectrolytes, charged amphiphiles^[14] and polypeptides.^[15]

The hPF-MD method has, therefore, been around for a decade, and its capabilities and shortcomings are well-known. We will discuss them in this contribution only, as far as needed for our redevelopment, and otherwise refer the reader to the existing literature.^[2,5,7,8,15] For various types of soft matter, the structural properties in are usually well reproduced hPF-MD, with the exception of very small-scale structures, such as the short-range part of a radial distribution function. The soft interactions of the density-functional-field, however, eliminate the mechanisms, which are necessary for the correct dynamics. For example, polymer chains are able to interpenetrate mutually due to the absence of excluded-volume interactions, as the *nonbonded* atom-atom interaction is effectively soft-core. This allows fast equilibration of polymer melts also for long chains, but precludes entanglements and reptation dynamics, rendering all dynamic properties, from diffusion to rheology, artificial, and qualitatively wrong.

The problem of incorrect chain crossability also arises in very CG polymer models, since from a certain degree of coarse-graining onward, interactions necessarily become soft-core.^[1] To recover the chain entanglements in simulations with such soft *nonbonded* interactions, several attempts have been reported. Padding and Briels proposed an algorithm called TWENTANGLEMENT to detect and prevent chain-crossing events by including an additional interbond interactions in mesoscopic simulations of polymer melts.^[16,17] Similar attempts are also made by Pan and Manke to reduce the frequency of artificial chain segment crossing events in dissipative particle dynamics (DPD) simulation via introducing a segmental repulsive potential.^[18] Alternative methods have been developed to represent the uncrossability (entanglements) in molecular simulations. Schieber and coworkers demonstrated successive versions of discrete slip-link models for predicting the rheology of entangled polymer liquids and gels, where the chain is CG to the entanglement level and the dynamics of chains is split into chain sliding and constraint release.^[19,20] Due to the failure of the standard tube model in describing the experimental neutron spin-echo measurements, Likhtman introduced a new single-chain dynamic slip-link model (slip-spring hereafter) to describe the experimental results for neutron spin echo, linear viscoelasticity, and diffusion of monodisperse polymer melts.^[21] Along with the development of these single-chain models, several multi-chain models have been proposed. Shanbhag et al. presented a dual slip-link model for studying the relaxation of entangled star polymers with chain-end fluctuations and constraint release, which explained deviations observed in dielectric and stress relaxation experimental data. Later, Masubuchi et al. proposed a primitive chain network,^[22] in which the chains are dispersed in the space and connected by slip-links to form a network. This model is able to reproduce the linear and nonlinear viscoelastic properties of entangled polymer melts. However, it is not rigorous in terms of thermodynamical properties because the

free-energy description of the model has not been found. Inspired by the single-chain slip-spring model of Likhtman, Masubuchi and coworkers performed a series of multi-chain simulations where the entanglements are replaced by slip-springs instead of the excluded-volume interaction^[23-26] with an accurate description of the free energy in the system. Chappa et al.^[27] and Langeloth et al.^[28] in parallel proposed models incorporating the slip-springs with DPD simulations. The mean-square displacements (MSDs) of beads from their models are demonstrated in favorable agreement with the tube model predictions.^[27-29] Later, Ramírez-Hernández et al. reported a theoretically informed entangled polymer simulation approach. In their approach, the topological effects that arise from the noncrossability of molecules are introduced through effective fluctuating interactions, mediated by slip-springs, between neighboring pairs of polymer chains.^[30] Recently, Theodorou and coworkers^[31] developed a mesoscopic particle-field Brownian dynamics methodology for simulating polymeric materials in realistic time scales. In their approach, the CG beads consist of several Kuhn segments, and the entanglement effect is introduced by the slip-springs, similar to the previous work in this field.

Thus, multi-chain slip-springs have been shown in multiple circumstances to re-introduce the effect of entanglements into the dynamics of polymer chains for particle models too CG. This is where the second technique of our approach, namely slip-springs, comes in. We adopt our own slip-spring model, which has already been used successfully with DPD.^[28,29] Slip-springs are virtual harmonic bonds between monomers of two different polymer chains. These virtual bonds are not connecting segments of chains statically and permanently but they can move along the chains following a Monte-Carlo governed hopping dynamics. This naturally restricts lateral chain motion and facilitates the longitudinal one. The use of slip-springs with dissipative-particle dynamics is another proven technology, with its range of applicability well established.^[28,29,32] We will, therefore, not review its features in detail, but only to the extent needed for the combination with hPF-MD.

In this paper, we report, for the first time, a combination of hPF-MD with slip-springs, and we validate the performance of the combination of the two components. Those, we regard as established methods with their advantages and disadvantages well documented in the literature. In particular, we first check whether the addition of slip-springs changes any static structural properties of the hPF-MD method, or whether they can be combined safely. This is mainly done by comparing these results for hPF-MD simulation with and without slip-springs. Second, we study the capability of slip-springs to restore entangled dynamics to hPF-MD. To this end, we compare slip-spring hPF-MD calculations with both hPF-MD (no slip-springs) and reference traditional atomistic MD simulations, as far as we are able to afford them. An atomistic model of polyethylene (PE) is chosen as an example to examine the effectiveness of slip-springs in reproducing the entangled dynamics in hPF-MD simulations. Our slip-spring hPF-MD model demonstrates good reproduction of polymer structures compared to the reference MD simulations. Additionally, the topological entanglements as analyzed by the Z1 method^[33-35] are consistent

with those from MD simulations and the number of entanglements (kinks) per chain is in qualitative agreement with the chain-length dependent number of slip-springs in the long-chain region. Entangled behavior in translational and reorientational dynamics are characterized by MSDs, bond and end-to-end vector reorientational autocorrelation functions in multiple ways. The time scaling behavior clearly shows that reptation motion can be restored, whereas slight accelerations are found in the short-time regime in both translational and orientational dynamics. This serves to demonstrate that the new slip-spring hPF-MD combination is an alternative to traditional atomistic MD for the study of structural and dynamical properties of polymer systems, as it is much faster. Its well-controlled approximations maintain enough agreement with the reference calculation to be a useful tool.

2 | METHODOLOGY

2.1 | Model

In our model, the dynamics of the polymer system is divided into two parts: (1) Newtonian motion of atoms and (2) hopping movement of slip-springs. The Newtonian motions are governed by three types of forces: (a) bonded, (b) density-functional, and (c) slip-spring potentials. The *bonded* potentials such as bond, angle, and dihedral potentials are exactly the same as used in standard atomistic MD simulations, see below. The *nonbonded* interactions are calculated using the density-functional potential field of the hPF-MD model. For a system of different types of particles, the total interaction energy in the density field is

$$W[\rho(r)] = \frac{1}{\rho_0} \int dr \left(\frac{k_B T}{2} \sum_{ij} \chi_{ij} \rho_i(r) \rho_j(r) + \frac{1}{2\kappa} \left(\sum_i \rho_i(r) - \rho_0 \right)^2 \right) \quad (1)$$

where the Flory-Huggins parameter χ_{ij} represents the strength of the mean field interaction between particles of type i and j , ρ_0 is the average number density of the system, ρ_i and ρ_j are the number densities of particles of type i and j in the density field, respectively, and κ is the compressibility factor for the system. The density-functional potential acting on individual particles is obtained from the functional derivative of the total field interaction energy with respect to the local density which is given by:

$$U_i^{\text{field}}(r) = \frac{\delta W[\rho(r)]}{\delta \rho_i(r)} = \frac{1}{\rho_0} \left(k_B T \sum_j \chi_{ij} \rho_j(r) + \frac{1}{\kappa} \left(\sum_i \rho_i(r) - \rho_0 \right) \right) \quad (2)$$

Between lattice points, the potential is numerically interpolated, so that the *nonbonded* force acting on an atom at any point in this space can be calculated. More details about the density-functional potential and its implementation can be found in former publications.^[2,5,10–12,14,15]

A constant number of slip-springs is introduced to mimic the binary contacts of topological constraints between entangled strands, replacing chain noncrossability in hPF-MD simulations. As discussed in ref. [36], monomers of a Rouse chain are confined to a tube-like region by an effective harmonic potential formed by the neighboring chains. In this spirit, a harmonic bonding potential is employed for slip-springs in this work:

$$U_{\text{spp}}(r) = \frac{1}{2} K_{\text{spp}} (r - r_{0,\text{spp}})^2 \quad (3)$$

where r is the distance between two connected atoms, K_{spp} is the slip-spring force constant and $r_{0,\text{spp}}$ is the equilibrium distance of the slip-spring.

Initially, one end of each slip-spring is connected randomly to an atom. The other connected atom is chosen nearby under the distance criterion $\frac{1}{2} r_{0,\text{spp}} < r < 2r_{0,\text{spp}}$. Slip-springs are allowed to exist as interchain or intrachain, representing entanglements between different chains and self-entanglements, respectively. The movements of these interchain and intrachain slip-springs are controlled in the same way by a Metropolis Monte-Carlo scheme. The locations of slip-springs on atoms are frozen during the Newtonian motion of atoms, and they are mobile only in the intervening Monte-Carlo phases. In a single Monte-Carlo step, each slip-spring attempts to move by one monomer to the left or to the right along the backbone of either polymer chains with an equal probability. The move is accepted with probability $p = \min(1, e^{-\Delta U_{\text{spp}}/k_B T})$, where ΔU_{spp} is the difference of the slip-spring energy between the trial and the old configuration. For simplicity, the movements of slip-springs are completely independent of each other, which means they can pass through one another and one atom can host multiple slip-springs. This implementation is different to some recently developed slip-spring models which apply an excluded volume repulsion between slip-springs.^[30,37] It is, however, still not clear whether the excluded volume interaction of slip-springs makes a qualitative difference on the dynamics of polymer melts.^[23,27,28,30] In the rare event that two ends of a slip-spring are connected to the same monomer, this slip-spring is destroyed and recreated randomly elsewhere in the system to avoid the formation of entanglement knots. The influence of this annihilation behavior of slip-springs on the dynamics is negligible due to the extremely rare occurrence of this event. To model the disentanglement at chain ends and the constraint release mechanisms, we also introduced a relocation Monte-Carlo move: If one end of a slip-spring reaches the end of the polymer chain, it may be destroyed and recreated at another randomly chosen chain end in the system. The relocation move is accepted with probability $p = \min(1, e^{-\Delta U_{\text{spp}}/k_B T})$, where ΔU_{spp} is the difference of the slip-spring energy between the new trial slip-spring and the old one. Under this formalism, the lateral chain motion is strongly restricted by the interchain slip-springs, while the longitudinal motion of the chain along the contour remains allowed.^[28,29]

The time evolution of the simulation uses alternating MD and MC blocks. The atom positions are propagated by integrating the equation

of motion under NVT conditions over n_{MD} timesteps using a velocity-Verlet^[38] algorithm and a Nosé-Hoover^[39] thermostat. Between MD intervals, the configurations of slip-springs are renewed via n_{MC} Monte-Carlo trial moves described above. At the end of an MC block, the Hamiltonian for the subsequent MD has thus been altered. The simulation ends when the total simulation time (MD steps) is reached.

2.2 | Simulations details

We employ the same united-atom model of PE^[40] for performing reference MD simulations (denoted as MD in the following), hPF-MD simulations without slip-spring (hPF-MD), and slip-spring hPF-MD simulations. There are several advantages to choose this polymer model as our example. First, this study investigates structural and dynamical properties of PE melts with chain length N (number of carbons in the backbone) ranging from C_{150} to C_{2600} covering weakly to strongly entangled regimes. As a reference, the experimental entanglement length of PE melts is around $N = 85$.^[41] The study of entangled PE requires long simulation times to show the features of entangled dynamics. The choice of united-atom model of PE reduces the computing expense. Moreover, united atom models of PE have been used in a large body of literature investigating its structures, dynamics and rheology properties, and their relation to experiment.^[41–46] The force field of the united-atom model of PE is shown in Table 1. The atoms have no partial charges.

In the particle-field part, the lattice constant of the density grid is chosen as 2 Å which is close to the skeletal bond length 1.53 Å and the updating interval of density field is set to be 1 MD timestep to guarantee enough chemical details captured. At a melt density of ~ 0.77 g/cm³, a grid cell contains, on average, ~ 0.29 united atoms. As this contribution is focused on the interplay of hPF-MD and slip-springs, we use this rather fine grid to rule out approximation errors due to the numerics of the grid treatment, we deliberately forgo, for the moment, the possibility of coarser grids, which would effectively CG the *nonbonded* interactions and would further speed up the calculations.^[47] The Flory-Huggins parameter χ is 0 for homogeneous

polymer melts. The incompressibility factor $1/\kappa$ is chosen as 5 kJ/mol which is similar with previous studies.^[5,48] For a better description of the structural behavior of PE melts in hPF-MD simulations, we utilize an additional intramolecular Leonard-Jones potential for 1–5 interactions (Table 1), similar to that used in Monte-Carlo simulations of single polymer chain in melt states,^[49,50] whereas carbon atoms separated by more than four bonds only interact by the *nonbonded* interactions as modeled by the field.

In our slip-spring formalism, the confinement of a polymer chain to its tube is governed by a set of slip-spring parameters: n_{MD} and n_{MC} , K_{ssp} and $r_{0,ssp}$, and N_{ssp} . Generally, the mobility of slip-springs is determined by n_{MD} and n_{MC} , and the effect in our model is similar to the findings in the slip-spring-DPD simulation of entangled polymer melts.^[28,29] We choose $n_{MD} = 500$ time steps and $n_{MC}/n_{MD} = 1$ after testing several combinations of n_{MD} and n_{MC} . Recent MD simulations suggested that the distance of binary contacts in polymer entanglements is between $\frac{1}{2}\sigma$ and 2σ , where σ is the monomer diameter.^[51] We use a similar equilibrium distance for the slip-springs $r_{0,ssp} = 5.28$ Å, which is the distance of the first peak of the intermonomer radial distribution function. The collective localizing strength of the slip-springs should be strong enough to confine the polymer chains, but any single one should not be too strong, thus K_{ssp} is chosen to be 300 kJ/mol $\approx \frac{1}{5}K_b$. Hence, the number of slip-springs N_{ssp} per chain is the only variable remaining in our formalism. It is determined from the reference MD simulations. Specifically, we first conduct slip-spring hPF-MD simulations with varying number of slip-springs in the system. The number of slip-springs is then determined when the target property (MSDs in this work) of the slip-spring hPF-MD simulations matches that of the reference MD simulations. The resulting number of slip-springs per chain is found to be dependent on the polymer chain length in a linear relation (see details in Figure S2). The relation between N_{ssp} and the related topological entanglement statistics is discussed below.

All PE melts studied in this work are summarized in Table 2. The initial configurations of all systems except PE (C_{2600}) are taken from the reference MD simulations after the density of the systems has been converged. In the case of PE (C_{2600}), we take the density of PE (C_{1300}) and equilibrate the system by a hPF-MD simulation following

TABLE 1 United-atom force field for polyethylene^[40,46]

Force field	Analytical form	Parameters
Bond	$U_{\text{bond}}(r) = \frac{1}{2}K_b(r-r_b)^2$	$K_b = 1,463$ kJ/Mol, $r_b = 1.53$ Å
Angle	$U_{\text{angle}}(\theta) = \frac{1}{2}K_\theta(\theta-\theta_0)^2$	$K_\theta = 250.8$ kJ/Mol/rad ² , $\theta_0 = 109.5^\circ$
Dihedral	$U_{\text{dihedral}}(\phi) = \sum_{i=0}^3 C_i(\cos\phi)^i$	$C_0 = 7.26$, $C_1 = -18.77$, $C_2 = 3.24$, $C_3 = 29.21$ (kJ/Mol)
Pair	$U_{\text{LJ}}(r) = 4\epsilon \left[\left(\frac{\sigma}{r}\right)^{12} - \left(\frac{\sigma}{r}\right)^6 \right]$, $r < r_c$	$\sigma = 4.01$ Å, $\epsilon = 0.47$ kJ/Mol, $r_c = 10$ Å

TABLE 2 Systems of polyethylene melts studied

N	M	N_{ssp}	d (Å)
150	60	9.7	64.7
200	60	11.6	71.1
250	48	13.4	70.8
300	40	15.3	70.8
350	35	17.1	71.2
520	53	23.5	93.3
1,300	25	52.5	97.6
2,600	25	100.8	97.6

Abbreviations: N, number of carbon atoms; M, number of chains in the melts; N_{ssp} , number of slip-springs per chain; d, size of the simulation box.

the equilibration procedure introduced in ref. [19]. The MD time step δt is 1 femtosecond for all simulations. All simulations are performed in the NVT-ensemble at a temperature of 450 K, to ensure that the polymer is in the melt state and that neither crystallization nor vitrification occurs, using GPU-Accelerated Large-Scale Molecular Simulation Toolkit (GALAMOST)^[52] integrated with the in-house code of the slip-spring model.

3 | RESULTS AND DISCUSSION

3.1 | Structural properties

3.1.1 | Statistics of polymer chains

First, we compute the mean square distance $\langle R^2(s) \rangle$ between monomers separated by a number of bonds s along the backbone of polymer chains, as shown in Figure 1. Systems of the longest polymers (C_{2600}) in hPF-MD simulations with and without slip-springs reach the same characteristic distance $\langle R(s)^2 \rangle / s \approx l_0^2 C_\infty = 17.47 \pm 0.22 \text{ \AA}^2$, where l_0 is the skeletal bond length (1.53 \AA) and $C_\infty = 7.46 \pm 0.09$ is the characteristic ratio for the polymer with a given chemistry and temperature. As a reference, the PE characteristic ratio from experiments is $C_\infty^{\text{exp}} = 7.5 \pm 1.7 (423 \text{ K})$.^[53] The good overlap of the results from the hPF-MD simulations with and without slip-springs indicates that the conformations of the linear chain and the correlation between monomers are, as expected, not affected by the introduction of slip-springs. Compared to the MD results (C_{350}), an excellent reproduction can be seen for small and large numbers of bonds ($s < 50$ and $s > 200$) and a slight deviation (less than 5%) for intermediate number of bonds s which is due to the too weak short-range correlation provided by soft potential of density fields. It is, thus, a feature introduced by the hPF-MD approximation itself and not by the addition of slip-springs.

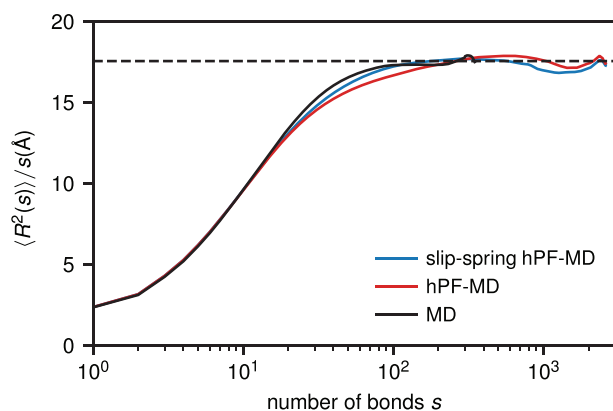


FIGURE 1 Normalized mean square distance between monomers of one chain as function of number of bonds s between them along the backbone for hPF-MD (red, PE- C_{2600}), slip-spring hPF-MD (blue, PE- C_{2600}), and MD (black, PE- C_{350}) simulations. The dashed line is the plateau value from the MD simulation [Color figure can be viewed at wileyonlinelibrary.com]

The probability distributions of the end-to-end distances $P(R_{\text{ete}})$, with C_{150} and C_{350} as examples, are shown in Figure 2. The coincidence of the probabilities at all length scales shows the good agreement of our model with the reference MD simulations on the structures. In theory, the mean-square radius of gyration (R_g^2) and the mean-square end-to-end distance (R_{ete}^2) of linear Gaussian polymer chains in the melt are linearly related to the chain length or molar mass, which is believed to be still valid in strongly entangled polymers. Figure 3 shows R_g^2 and R_{ete}^2 for different chain lengths of hPF-MD with and without slip-springs as well as reference MD simulations in a double-logarithmic scale. From the fits in Figure 3, we extract scaling exponents for R_g^2 and R_{ete}^2 , which are 1.01 and 1.01, respectively, numerically equal to 1. This is in excellent agreement with the

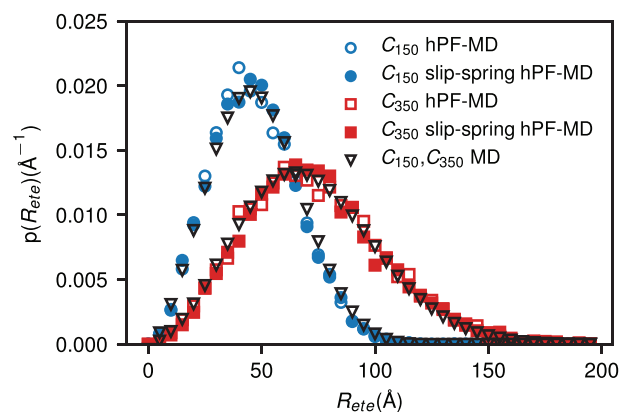


FIGURE 2 Distribution of end-to-end distance for polyethylene C_{150} (circles) and C_{350} (squares) in melts. Results from our hPF-MD (hollow), slip-spring hPF-MD (filled), and MD (black) simulations are compared [Color figure can be viewed at wileyonlinelibrary.com]

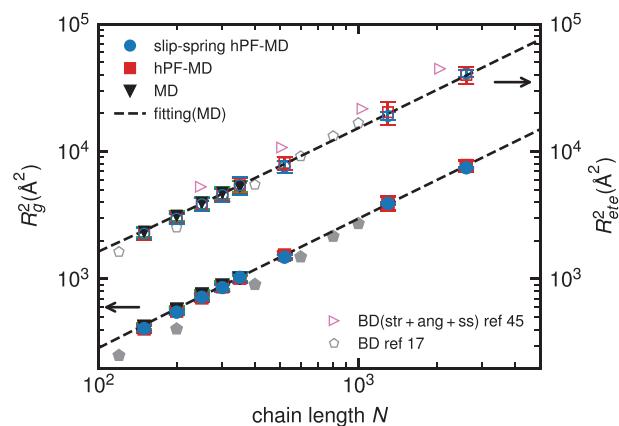


FIGURE 3 Dependence of radius gyration R_g^2 (filled, left axis) and end-to-end distance R_{ete}^2 (hollow, right axis) on the chain length N . Results from hPF-MD (red), slip-spring hPF-MD (blue), and MD (black) simulations are compared. These results are compared with the Brownian dynamics simulations of long polyethylene chain (pink triangles^[45] and gray pentagons^[17]). Dashed lines are the power law fits for the MD results [Color figure can be viewed at wileyonlinelibrary.com]

theoretical predictions. Furthermore, R_g^2 and R_{ete}^2 are separated by a factor of 6.01 for long PE chains, which is very close to the value of 6 predicted for Gaussian chains. The MD values of both the radius of gyration and end-to-end distance of short chains (C_{150} , C_{350}) are reproduced very well by the hPF-MD simulations with and without slip-springs. For long PE chains (C_{520} , C_{1300} , C_{2600}), the configurations of PE chains still follow the scaling law which is extrapolated from our MD results. The good reproduction of both R_g and R_{ete} compared with reference MD simulations shows the validity of our slip-spring hPF-MD simulations for structural properties, which is consistent or even better than the original hPF-MD model.^[5,48] The configurations of polymer chains do not change with the introduction of slip-springs. This further confirms that slip-springs do not alter the equilibrium properties the polymers. It is worth noting that the impact of slip-springs on the statistics of polymer chains may depend on the incompressibility condition (κ in Eq. (2)) of our system. Specifically, if the compressibility factor κ is large, which means that the system is compressed more easily, the additional interactions of the slip-springs may in principle cause contraction of the polymer chains. With the current combination of parameters, though, this is evidently not the case.

3.1.2 | Topological entanglement analysis

The phenomenological tube model assumes that a long polymer chain is confined to a tube-like region and it is only allowed one-dimensional reptational motion along it.^[54,55] Numerous studies have tried to find a microscopic definition of topological confinements or entanglements.^[35,51,56–58] One can analyze the topological entanglements by means of contour-length minimization or chain-shrinking for the polymer chains via CReTA^[57] and Z1^[33–35] algorithms. In brief, these algorithms construct primitive paths (PP) by fixing the chain ends in space and minimizing their contour-lengths without allowing chains to cross each other. This means that the excluded volume effect is preserved to avoid chain-crossings. The statistics of the topological constraints such as the entanglement length N_e is believed to be closely related to dynamical analysis and rheological measurements according to the tube model.^[56] Results calculated on the same configuration using CReTA and Z1 are found almost identical. As the Z1 algorithm converges faster and is more efficient for large systems,^[35] we choose it in this work to further investigate structural differences between MD and hPF-MD simulations in terms of topological entanglements and the configurational effect of slip-springs in hPF-MD simulations. It is worth noting that the statistics of topological entanglements obtained from Z1 code in hPF-MD simulations with and without slip-springs is calculated only from single, static configurations, without recourse to entangled dynamics. In theory, polymer chains could cross each other in pure hPF-MD simulations, if we fixed the chain ends and minimized the chain length, and the final contour length would simply be the end-to-end distance. In the Z1 analysis, we impose chain uncrossability, even if in the parent hPF-MD simulation the chains were allowed to cross. In systems with the slip-spring

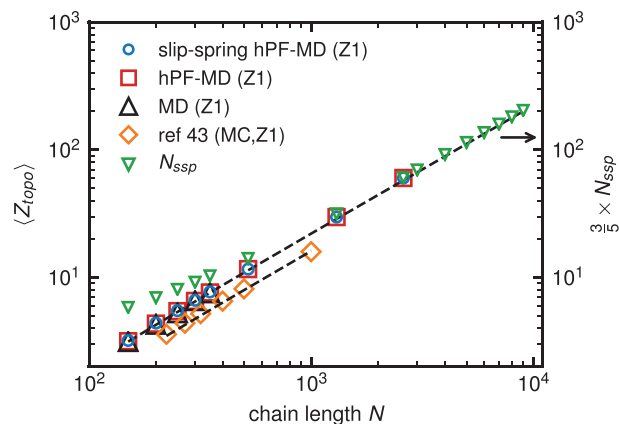


FIGURE 4 Dependence of the average number of topological entanglements per chain ($\langle Z_{topo} \rangle$) (left axis) on the chain length N . $\langle Z_{topo} \rangle$ from our hPF-MD (red), slip-spring hPF-MD (blue), and MD (black) as well as other simulation results (orange)^[43] are compared. Number of slip-springs per chain N_{ssp} (right axis, green) is compared with $\langle Z_{topo} \rangle$. Dashed lines are the linear fit of $\langle Z_{topo} \rangle$ of our MD results with slope ~ 0.02 [Color figure can be viewed at wileyonlinelibrary.com]

hPF-MD model, the slip-springs are interpreted as topological entanglements which are identical to “kinks” in Z1 code. Here, the contour length can be calculated by summing up the distances between chain-ends and segments connected by slip-springs.

The number of entanglements (kinks) per chain ($\langle Z_{topo} \rangle$) and the slip-springs per chain N_{ssp} are plotted as a function of N in Figure 4. Both $\langle Z_{topo} \rangle$ and N_{ssp} are proportional to the polymer chain length in general. The overall good agreements between MD and hPF-MD simulations are observed by the overlap between symbols of $\langle Z_{topo} \rangle$. These observations indicate that hPF-MD simulations with soft *non-bonded* interactions can generate configurations of entangled melt similar to the standard MD with hard-core interactions. Furthermore, the introduction of slip-spring does not affect the statistics of topological entanglements at all. Moreover, comparing to Monte-Carlo simulations of PE melts by Kröger et al.,^[43] who used a united-atom model at 450 K, our simulation results are seen in good qualitative agreement with theirs, although slightly larger. If the N_{ssp} are multiplied by 0.6 (Figure 4, right axis), they coincide with the topological entanglements $\langle Z_{topo} \rangle$ in well-entangled PE melts. Thus, for long enough chains, each slip-spring is comparable to 1.67 topological entanglements (kinks) in the Z1 analysis, while in short chains ($C < 1,000$), each slip-spring is comparable to fewer topological entanglements.

The entanglement length N_e is defined through:

$$N_e = (N - 1) \frac{\langle R_{ete}^2 \rangle}{\langle L_{pp} \rangle^2} \quad (4)$$

where the bracket indicates the ensemble average and L_{pp} represents the primitive path length. This definition of N_e is denoted as classical

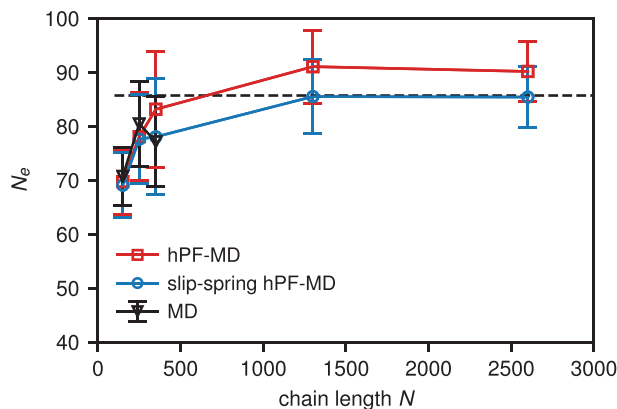


FIGURE 5 Dependence of entanglement length N_e computed by the Z1 code on the chain length N . Results of N_e from hPF-MD (red), slip-spring hPF-MD (blue) and MD (black) are compared. The dashed line is the entanglement length for polyethylene melts from the experiment^[59] [Color figure can be viewed at wileyonlinelibrary.com]

S-coil in the Z1 code.^[34,43] In Figure 5, the entanglement length N_e from the Z1 analysis shows asymptotic behavior in all simulations. It increases with the chain length and reaches a plateau for long chains. Good agreement is observed between MD and hPF-MD results, indicating the good reproduction of the topological entanglement, even though the excluded volume is imposed only postsimulation at the analysis stage (Z1 algorithm). For comparison, the entanglement length N_e of long enough polymer chains from the hPF-MD simulations with ($N_e = 85.7 \pm 5.9$) and without slip-springs ($N_e = 90.2 \pm 6.2$) is found to be close to the experimental entanglement length $N_e = 85.7$, the value of which was calculated from the plateau modulus of ultrahigh-molecular-weight PE in the melt state at temperature $T = 463$ K.^[41,59] It is notable here that the entanglement length computed by the Z1 code is not initially aimed to be quantitatively comparable to the experimental measurements due to the different methods (definitions) used for its determinations, although the molecular weight dependence of N_e was estimated in prior experimental studies.^[60,61] The slip-spring hPF-MD entanglement length appears to be systematically shorter than the pure hPF-MD values for the three longest chains by about 10%, thereby being in closer agreement with the experiment. It is at present not clear whether this fact is coincidental or whether the introduction of slip-springs preconfigures the melt conformations to have more topological entanglements.

3.2 | Translational dynamics

The diffusive motion of entangled polymers has been well investigated by both experiments and molecular simulations.^[42,62–66] In well-entangled polymer melts of very long chains, the MSD of the central monomers $g_1^{\text{mid}}(t)$ should show five distinct regimes corresponding to the different underlying relaxation mechanisms, which are postulated by the tube model. The corresponding scaling behaviors are

$$g_1^{\text{mid}}(t) \approx \begin{cases} C_0 t^2, & t < \tau_b \\ C_1 t^{1/2}, & \tau_b < t < \tau_e \\ C_2 t^{1/4}, & \tau_e < t < \tau_R \\ C_3 \frac{t^{1/2}}{N^{1/2}}, & \tau_R < t < \tau_d \\ C_4 \frac{t}{N^2}, & \tau_d < t \end{cases} \quad (5)$$

where C_0 , C_1 , C_2 , C_3 , and C_4 are phenomenological parameters. One can then determine the characteristic times: ballistic time τ_b , entanglement time τ_e , Rouse time τ_R , and terminal (disentanglement) time τ_d by the intersections between the power-law fits of different regimes.

PE united-atom models of C_{150} – C_{350} are simulated by all methods and longer chains (C_{520} – C_{2600}) are only simulated by hPF-MD simulations with and without slip-springs. Within the time scale simulated, good agreement with the theoretical predictions (Equation 5) is clearly seen (Figure 6) for the MD simulation data and excellent reproduction of the entangled dynamics is found for the slip-spring hPF-MD model. The characteristic time from free Rouse motion to constrained Rouse motion τ_e is shifted due to the low monomeric friction from the soft-core particle-field potentials in the hPF-MD model.

Figure 6 generally shows three different representations of the MSD of the central monomers of the polymer chain. The choice of central monomers excludes the effect of chain ends, which gives better agreements when comparing with the tube model.^[66,67] Note that no phenomenological or empirical shifting has been performed on the curves in Figure 6. In Figure 6a, the normal MSDs from our MD and hPF-MD simulations span around 10 orders of time which makes it difficult to see clear characteristic behaviors and differences between them. Figure 6b,c shows the same data but rescaled with $t^{0.5}$ and $t^{0.25}$ which reduces the range of the vertical axis to around 6 orders and exposes the differences among them, allowing clearer comparisons with the scaling predictions of the tube model. In theory, the free Rouse motion ($\tau_b < t < \tau_e$) is seen as plateau in the representation of g_1^{mid} rescaled with $t^{0.5}$ (Figure 6b) and the constrained Rouse motion (entangled dynamics, $\tau_e < t < \tau_R$) is seen as a deep depression. In Figure 6c,d where g_1^{mid} is rescaled by $t^{0.25}$, the constrained Rouse motion is observed as a horizontal plateau. In the following, we mainly focus on the rescaled representations of the MSD.

The monomer MSDs of PE with different chain lengths follow a universal behavior in the ballistic regime ($t < \tau_b$). Above τ_b , theoretically, the polymer segments conduct free Rouse motion ($\tau_b < t < \tau_e$). Our MD and pure hPF-MD results reproduce this behavior (Figure 6b), but the latter is significantly faster. The acceleration seen in pure hPF-MD simulations is not surprising because the friction is reduced due to the softness of the particle-field potential, consistent with previous hPF-MD studies.^[5,48] Polymer segments begin to feel confinements from the neighboring chains at τ_e , which is 2 ns for MD simulations, entering the constrained Rouse regime ($\tau_e < t < \tau_R$). Due to the absence of entanglements, τ_e does not exist in pure hPF-MD simulations. As seen in Figure 6c, no depression can be found, indicating that only free Rouse motions exist there. For slip-spring hPF-MD, in contrast, no long and stable plateau is seen in Figure 6b, which

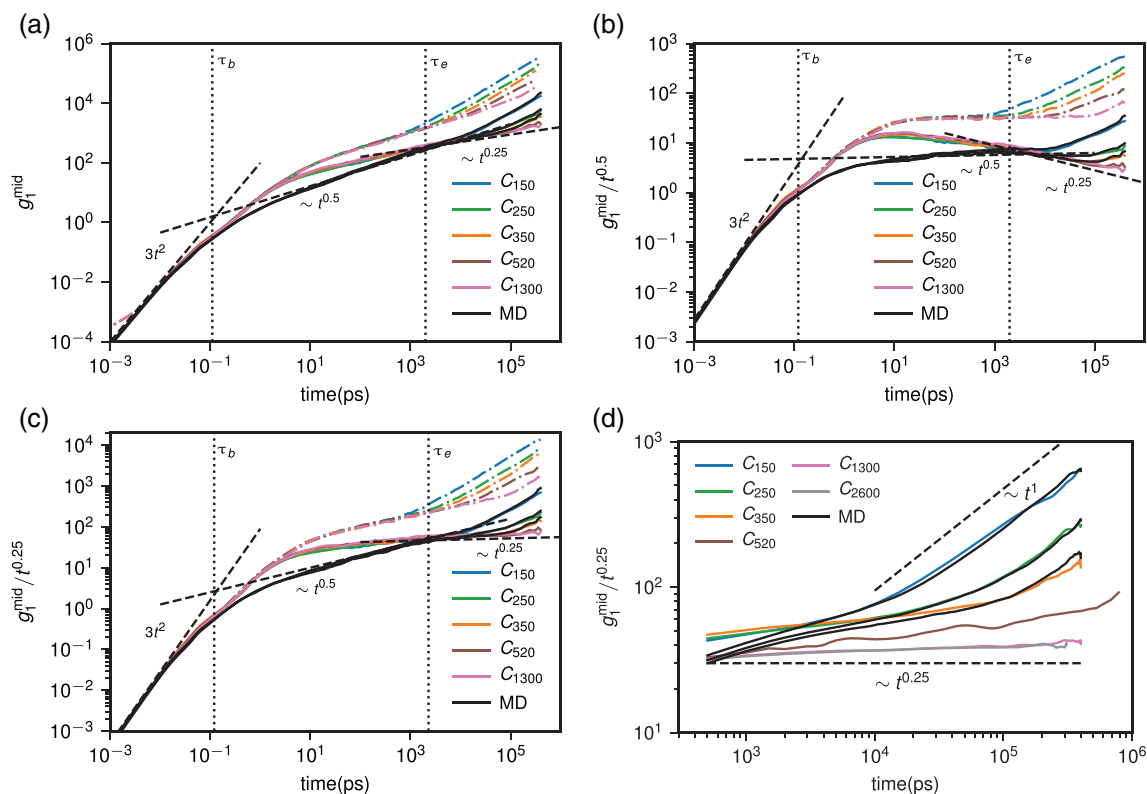


FIGURE 6 Mean square displacements of central monomers from hPF-MD (dot dashed lines), slip-spring hPF-MD (solid lines), and MD (black solid lines) simulations, (a) raw data, (b) rescaled by $t^{0.5}$ power law, (c) rescaled by $t^{0.25}$ power law, and (d) zoom on the reptation regime. The dashed lines are regimes postulated by the tube model for ballistic ($t < \tau_b$), free Rouse motion ($\tau_b < t < \tau_e$) and constrained Rouse motion ($\tau_e < t < \tau_R$) regimes. The vertical dotted lines are borders between two regimes, which are the characteristic time for polyethylene melts [Color figure can be viewed at wileyonlinelibrary.com]

means that free Rouse motion is barely taking place and the constrained Rouse regime begins early. These well-developed constrained Rouse motions are evident as the horizontal plateau in Figure 6c. The coincidence of the curves of $g_1^{\text{mid}}/t^{0.25}$ in Figure 6d demonstrates the good agreement of MSDs beyond $\tau_e \approx 2$ ns between the reference MD and the slip-spring hPF-MD simulations. This is a strong indication of the effectiveness of the slip-spring model to restore entangled dynamics to pure hPF-MD simulations. At the same time, the stable plateaus in this representation exhibit the expected $t^{0.25}$ scaling behavior for long polymer chains. In contrast, the acceleration of hPF-MD with respect to the reference MD simulations at short times ($\tau_b < t < \tau_e$) is still observed after introducing slip-springs, suggesting that the slip-springs impose constraints on the dynamics at the length and time scales of the entire polymer chain, rather than alter the local segmental dynamics. It should be noted here that the apparent coincidence of segmental MSDs between the classic MD and the slip-spring hPF-MD simulations are only statistical at long times in the time range which is computationally accessible for mildly entangled polymers ($N_C < C_{520}$) in this work.

The entanglement effects can also be identified through the ratios of MSDs of the end and center of a chain $g_1^{\text{end}}/g_1^{\text{mid}}$ (Figure 7). For an ideal well entangled linear Gaussian chain, the diffusion of the end

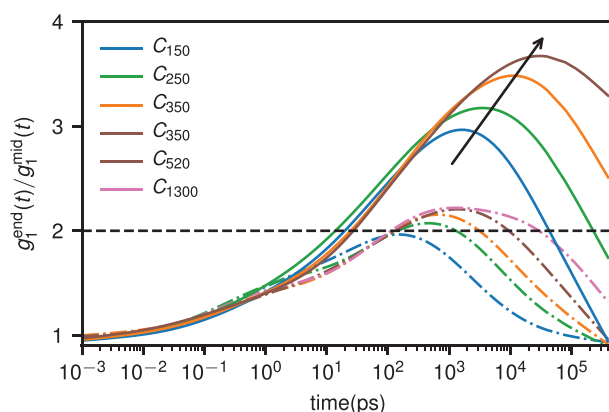


FIGURE 7 Ratios of the monomer mean square displacements of chain end and center, $g_1^{\text{end}}/g_1^{\text{mid}}$ from hPF-MD (dot dashed lines) and slip-spring hPF-MD (solid lines) simulations. The dashed line refers to the Rouse model prediction of $g_1^{\text{end}}/g_1^{\text{mid}} = 2$ at the intermediate time regime [Color figure can be viewed at wileyonlinelibrary.com]

and central monomers is similar below the ballistic time τ_b , since it is only affected by the background friction. In this stage $g_1^{\text{end}}/g_1^{\text{mid}} = 1$. Upon entering the free Rouse regime ($\tau_b < t < \tau_e$), the diffusion of the

monomers is not only influenced by the background friction, but also by the bond connectivity of the chain. Chain end monomers are only connected to one piece of the chain, resulting in less restriction than for the central monomers of the chain. Thus, during this period, the $g_1^{\text{end}}/g_1^{\text{mid}}$ curve increases with time and is expected to reach the Rouse model value of 2 at $t = \tau_e$ in principle. Above $t = \tau_e$, the motion of the central monomers starts to feel the topological confinements from the neighboring chains, while the chain ends are still free to move to take part in the tube renewal. The $g_1^{\text{end}}/g_1^{\text{mid}}$ curve keeps increasing and, at $t = \tau_R$, it is predicted according to the tube model to reach a maximum value. After that, the entire chain starts to move coherently and fully diffuses around the terminal time τ_d . In this regime, the $g_1^{\text{end}}/g_1^{\text{mid}}$ curve decays back to 1. For the result in Figure 7, we take 10 monomers from chain center and the outermost 5 monomers at each chain end as our samples. The curves have been smoothed by a spline interpolation for better visualization. The hPF-MD simulations with and without slip-springs share the same qualitative trend. Particularly, at $t < 10$ ps, the $g_1^{\text{end}}/g_1^{\text{mid}}$ curves are well overlapped. However, the maximum values of pure hPF-MD simulations do not increase much with the chain length, they seem to reach their maxima around $t \approx 2$ ns with $g_1^{\text{end}}/g_1^{\text{mid}} \approx 2.1$. For slip-spring hPF-MD simulations, the $g_1^{\text{end}}/g_1^{\text{mid}}$ curves increase faster and reach their maxima later than for pure hPF-MD simulations. These obvious differences after introducing slip-springs confirm the ability of the slip-springs to better confine the motion of the chain centers. Moreover, the maximum value of $g_1^{\text{end}}/g_1^{\text{mid}}$ slip-spring hPF-MD increases with the chain length, consistent with the previous Monte-Carlo and MD simulations and the theoretical predictions for entangled polymers.^[62,67,68]

We also extract the maxima of the peaks in Figure 7 and plot them together with the theoretical predictions of the tube model as function of $\langle Z_{\text{topo}} \rangle^{-\frac{1}{2}}$, as seen in Figure 8. The number of entanglements per chain $\langle Z_{\text{topo}} \rangle$ used in this plot is the one computed by the

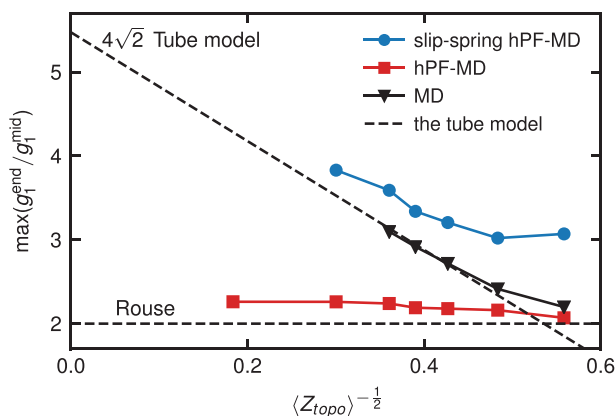


FIGURE 8 Dependence of maximum of the ratio $g_1^{\text{end}}/g_1^{\text{mid}}$ from hPF-MD (red), slip-spring hPF-MD (blue), and MD (black) simulations on $\langle Z_{\text{topo}} \rangle^{-\frac{1}{2}}$. The dashed line is the theoretical prediction of Rouse model and the tube model [Color figure can be viewed at wileyonlinelibrary.com]

Z1 code (see above). A value of $\max(g_1^{\text{end}}/g_1^{\text{mid}}) = 4\sqrt{2}$ is predicted theoretically from the Evans-Edwards model for polymers with infinite entanglements Z_{∞} .^[68] In the pure hPF-MD simulations, the maximum values of the $g_1^{\text{end}}/g_1^{\text{mid}}$ remain close to the Rouse prediction of 2 and for all $\langle Z_{\text{topo}} \rangle$. This means that only the Rouse behavior is found and entanglement effects are absent in the pure hPF-MD model for all chain lengths. By introducing slip-springs into the hPF-MD model, in contrast, the maxima clearly increase with $\langle Z_{\text{topo}} \rangle$, qualitatively consistent with the theoretical predictions of the tube model. This shows once more the capability of slip-springs to mimic the topological constraints in the hPF-MD model. There are, however, discrepancies between the tube model predictions and the slip-spring hPF-MD, which are probably owed to the different descriptions of the polymer model. An ideal Gaussian chain is assumed in the tube model, while in our simulations, an atomistic model with stronger chain rigidity is adopted.

The diffusion coefficients have also been estimated^[69,70] from linear regime of the MSD curve ($t > t_d$). According to the Rouse and tube model, the diffusion coefficient D of a linear entangled polymer melt system follows the scaling behavior given by:

$$D \sim \begin{cases} N^{-1}, & N < N_e \\ N^{-2}, & N > N_e \end{cases} \quad (6)$$

Figure 9 plots chain-length dependent diffusion coefficients. The diffusion coefficients from the pure hPF-MD simulations (red squares) scale approximately with N^{-1} , which shows no signature of reptation and is consistent with the chain-crossings allowed by the soft density-field interactions. In contrast, for the hPF-MD simulations with slip-springs, D scales with $N^{-2.03}$ for $N > N_e$, indicating the recovery of

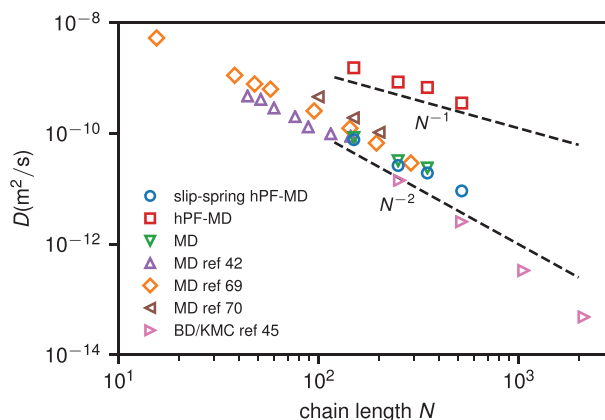


FIGURE 9 Scaling behavior of the diffusion coefficients with respect to the chain length. For hPF-MD simulations (red squares), $D_{\text{hPF}} \sim N^{-1}$; For slip-spring hPF-MD simulations (blue circle), the diffusion coefficients scale with N^{-2} ; The results are compared with our MD simulations (green inverted triangle) and other MD simulations of polyethylene melts (purple triangles,^[69] orange diamonds,^[42] brown triangles,^[70] and pink triangles^[71]). The dashed lines are guide lines to the eye [Color figure can be viewed at wileyonlinelibrary.com]

entangled dynamics. We also note that D from the slip-spring hPF-MD simulations is very close to the atomistic MD calculations of us and others quantitatively, the deviations of which may be attributed to the low statistics at long times needed for calculating the diffusion coefficients.

3.3 | Orientational dynamics

Polymer dynamics can also be measured in terms of orientational autocorrelation functions of various intrachain vectors. In well entangled polymers, the decay of the segmental orientational autocorrelation functions is significantly slowed by the entanglements. These retardations in orientational dynamics have been observed in NMR and dielectric spectroscopy^[72–77] and molecular simulations.^[67,78] In MD simulations, the normalized orientational auto-correlation functions are calculated as:

$$\text{ACF}(t) = \langle \vec{u}(t) \cdot \vec{u}(0) \rangle \quad (7)$$

where $\vec{u}(t) = \vec{l}(t)/|\vec{l}(t)|$ is the segmental unit vector with $|\vec{l}(t)|$ being the segment length at time t and the bracket denotes the ensemble average. The shortest $\vec{l}(t)$ is the backbone bond vector, which samples the local segmental dynamics. The longest is the end-to-end vector, which is only fully relaxed at the disentanglement time τ_d in entangled polymers. The relaxation time of the end-to-end vector τ_{ete} is the longest single-chain relaxation time in entangled polymer melts. In the Doi-Edwards tube model, τ_{ete} is predicted to be proportional to the third power of the chain length of entangled polymers N , while in experiments this characteristic exponent is measured as $N^{3.4}$. The deviation is interpreted by the other two underlying relaxation mechanisms: contour length fluctuation and constraint release which

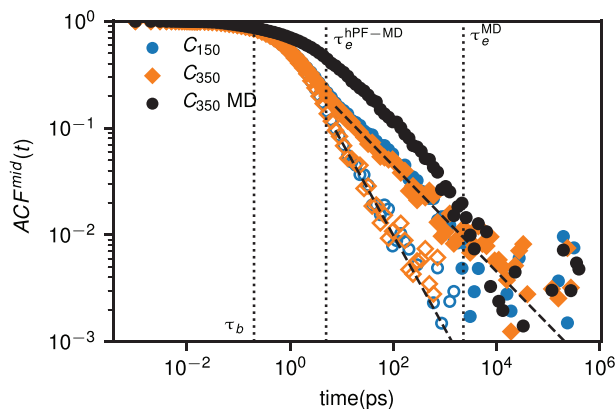


FIGURE 10 Bond orientational autocorrelation function averaged over the 50 bond vectors in the central chain from hPF-MD (hollow), slip-spring hPF-MD (filled), and MD (black) simulations of PE-C₁₅₀ and PE-C₃₅₀. Dashed lines are the exponential fitting for hPF-MD simulations with and without slip-springs [Color figure can be viewed at wileyonlinelibrary.com]

accelerate the disentanglement process and have been widely discussed.^[55,79–82] Since in our slip-spring model, the implementation naturally includes these two relaxation mechanisms besides reptation, the molecular weight dependence of τ_{ete} is expected to approach the experimental value.

Figure 10 exhibits the next-neighbor bond orientational auto-correlation function for various chain lengths in MD, hPF-MD and slip-spring hPF-MD simulations. The results are averaged over 50 bond vectors in the central part of the chain. Generally, the developments of the ACF function are similar to the translational diffusion characteristics, which can be distinguished with several characteristic times (τ_b , τ_e ...). As seen in the figure, the curves coincide in the ballistic regime ($t < \tau_b$), afterward they are separated and show different decay rates. The hPF-MD simulations with and without slip-springs share the same behavior up to $t \approx 10$ ps, which is consistent with findings in the MSDs, indicating that slip-springs do not alter the short-time segmental-orientation behavior either. After this time, the hPF-MD simulations with and without slip-springs deviate and the deviation increases with time. Discrepancies between MD and both hPF-MD simulations starts above the ballistic time $\tau_b \approx 0.5$ ps. Above $\tau_e^{\text{MD}} \approx 2$ ns, the ACF of slip-spring hPF-MD coincides again with that from MD simulations within the fluctuation of the data. Overall, the transition around the characteristic times ($\tau_b \approx 0.5$ ps, $\tau_e^{\text{hPF}} \approx 10$ ps and $\tau_e^{\text{MD}} \approx 2$ ns) is consistent with that of the MSDs g_1 shown above. This consistency implies that our slip-spring model influences translational and orientational segmental dynamics in the same way.

The other limit of single-chain relaxation time is that of the end-to-end vector, τ_{ete} , which can be estimated from the autocorrelation function of the end-to-end unit vector $\text{ACF}_{ete}(t)$. The autocorrelation

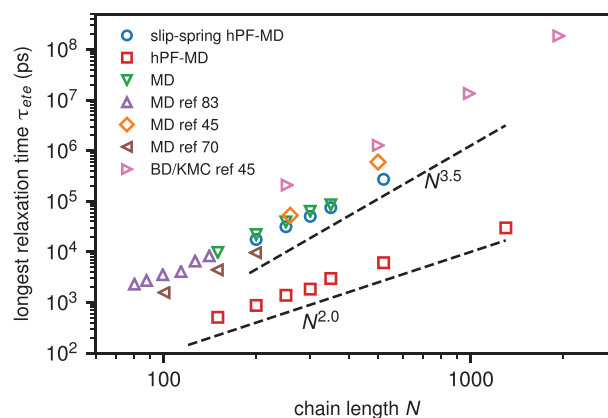


FIGURE 11 Results of relaxation time of end-to-end vector τ_{ete} as function of the chain length N from hPF-MD (red), slip-spring hPF-MD (blue), and MD (black) simulations. These results are compared with other molecular dynamics simulations (purple triangle,^[83] orange diamond,^[45] brown triangle^[70]), and equation of state Brownian dynamics simulation (pink triangle^[45]). The dashed lines are a guide to the eye which are power law scaling ($\tau_{ete} \sim M^{3.5}$) of entangled dynamics observed in experiments and scaling ($\tau_{ete} \sim M^{2.0}$) of unentangled Rouse behavior [Color figure can be viewed at wileyonlinelibrary.com]

function is expected to show exponential decay at long times when $ACF_{ete}(t)$ is smaller than a certain value (i.e., $1/e$). An exponential fit to this regime

$$ACF(t) = \exp\left[-\left(\frac{t}{\tau_{ete}}\right)\right] \quad (8)$$

yields τ_{ete} as a fit parameter. As discussed above, the Rouse model predicts $\tau_{ete} \sim N^2$ in unentangled polymer melts. The dependence of the relaxation time of end-to-end vectors τ_{ete} on the chain length of entangled PE chain from MD, hPF-MD simulations with and without slip-springs is shown in Figure 11. For the hPF-MD simulations, τ_{ete} is found to follow the Rouse prediction $\tau_{ete} \sim N^2$ for all chain lengths examined. With addition of the slip-springs, the chain reorientational mobility also slows down and its scales roughly as $\tau_{ete} \sim N^{3.5}$ in the limit of long chains, once more indicating the recovery of the reptation motions by the introduction of slip-springs. In passing, we note that the relaxation of the end-to-end vector is related to the stress relaxation in polymer melts.^[78,82,84,85] Since slip-spring hPF-MD reproduces the relaxation behavior of fully atomistic MD, it should offer a way to obtain, in principle, rheological properties of polymer melts. This is an interesting prospect, not yet pursued in this contribution, for obtaining rheological properties from hPF-MD. The traditional MD route via the Green-Kubo relation $G(t) = V \langle \sigma_{\alpha\beta}(t)\sigma_{\alpha\beta}(0) \rangle / k_B T$ from the stress fluctuation in equilibrium melts, does not work in hPD-MD since a rigorous prescription for calculating the stress tensor components $\sigma_{\alpha\beta}(t)$ for the particle-field terms has not (yet) been worked out.

4 | CONCLUSIONS

This work shows that the combination of multi-chain slip-springs with hybrid particle-field-MD (hPF-MD) simulations reproduces most aspects of entangled dynamics in polymer melts at atomistic resolution. The hybrid particle-field simulation is known for its computational efficiency compared to classic MD simulations. The combination with slip-springs inevitably requires additional computations. The calculation of slip-spring forces is in fact adds a small number of terms to the bond forces, and is thus cheap. The most demanding part is the neighbor search in relocation step. However, it takes place only infrequently through the whole simulation. As a consequence, the speed of the hybrid particle-field simulation with slip-springs reaches around 75% of the unmodified hPF-MD simulations for systems composed of up to 5×10^5 particles in the current serial implementation of slip-spring Monte-Carlo movements. The slip-springs successfully replace the topological constraints and efficiently offset the chain crossings inherent in hPF-MD models. Static polymer properties are reproduced well by hPF-MD simulations with and without slip-springs such as the chain conformations and primitive path statistics. Correct static structure calculations are not necessarily found in other single-chain or multi-chain slip-spring models.^[23,86] In addition, the detailed comparisons of the equilibrium structural properties between hPF-MD with and without slip-springs indicate that

the introduction of slip-springs alters neither the chain statistics nor the topological entanglements, even though no additional correction potential is utilized. This suggests that, at least for polymer melts, the interactions from the density-field are sufficient to sustain the polymer configurations, similar as for the DPD model reported earlier.^[28,29] This is an advantage of our slip-spring hPF-MD model over some other slip-spring models.^[23,27]

The unmodified hPF-MD ignores chain noncrossability and leads to a polymer mobility which is not only too fast, but also qualitatively wrong. Introducing slip-springs restores correct polymer dynamics on almost all time scales as has been shown in the analysis of monomer MSDs and bond orientational autocorrelation functions. These results are rather close to reference MD calculations with full pairwise interactions, especially above the entanglement time $\tau_e \approx 2$ ns. The impact of slip-springs is similar on translational (MSDs) and reorientational motion (bond auto-correlation functions) and scaling cross-overs occur at the same characteristic times. Moreover, with slip-springs present, the end-to-end relaxation time τ_{ete} obeys the same power law relation to molar mass of PE, as seen in experiments and MD simulations, whereas the end-to-end relaxation time τ_{ete} of unmodified hPF-MD follows the Rouse-law for all molar masses. The entanglement effect however emerges at relatively short times in slip-spring hPF-MD simulations and the Rouse-like regime is compressed and hardly seen in either segmental translational or orientational characterizations. Thus, slip-springs seem to alter the dynamics at intermediate time and length scales. The dynamics at this scale, however, might be separately addressed, if needed, via modifying the equations of motion such as employing Langevin or Lowe-Andersen dynamics. For $t < \tau_e$, the dynamics is Rouse like and the motions are governed by the monomeric frictions in three dimensions ζ_{3D} ,^[54,55,87,88] which has also been shown in CG polymer simulations.^[89]

We seem to have found a working combination of the control parameters of the slip-springs. Yet, the underlying physics of some parameters such as the ratio of MD to MC steps and the number of slip-springs used in our present formalism may need further investigations. The MD/MC ratio has been found to impact the diffusion behavior in a similar way in a previous model proposed by our group,^[28,90] namely by altering the effective Rouse time in one dimension (reptation) $\tau_{R,1D}$. This time is related to the one dimensional segmental friction coefficient ζ_{1D} ^[88] which is different from its three-dimensional counter part ζ_{3D} . Furthermore, the multi-chain slip-spring formulation and its incorporation with hPF-MD allow applications of the present model to problems specifically where the chemical details and intermolecular interactions have significant influences such as kinetics in complex morphologies of multicomponent polymeric materials^[91–93] and dispersions of nanoparticles into polymer matrices.^[94,95]

ACKNOWLEDGMENTS

Z. Wu thanks Prof. Martin Kröger for providing the Z1 code. The authors also thank our partners in the ROBERTO consortium (Prof. Toshihiro Kawakatsu and Prof. Yuichi Masubuchi) for many fruitful discussions along the project. This research is funded by the Deutsche

Forschungsgemeinschaft via the SFB-TRR 146 "Multiscale Simulation Methods for Soft Matter Systems", Project A8. Z. Wu gratefully acknowledges the computing time granted on the supercomputer Mogon at Johannes Gutenberg University Mainz. Open access funding enabled and organized by Projekt DEAL.

ORCID

Zhenghao Wu  <https://orcid.org/0000-0003-2862-4432>

REFERENCES

- [1] F. Müller-Plathe, *ChemPhysChem* **2002**, 3(9), 754.
- [2] G. Milano, T. Kawakatsu, *J. Chem. Phys.* **2009**, 130(21), 214106.
- [3] M. W. Matsen, M. Schick, *Phys. Rev. Lett.* **1994**, 72(16), 2660.
- [4] F. Drolet, G. H. Fredrickson, *Phys. Rev. Lett.* **1999**, 83(21), 4317.
- [5] A. De Nicola, T. Kawakatsu, G. Milano, *J. Chem. Theory Comput.* **2014**, 10(12), 5651.
- [6] S. Caputo, A. De Nicola, G. Donati, A. David, G. Raos, G. Milano, *J. Electrochem. Soc.* **2019**, 166(9), B3309.
- [7] A. De Nicola, Y. Zhao, T. Kawakatsu, D. Roccatano, G. Milano, *J. Chem. Theory Comput.* **2011**, 7(9), 2947.
- [8] G. Milano, T. Kawakatsu, A. D. Nicola, *Phys. Biol.* **2013**, 10(4), 045007.
- [9] G. J. Sevink, F. Schmid, T. Kawakatsu, G. Milano, *Soft Matter* **2017**, 13(8), 1594.
- [10] A. De Nicola, S. Hezaveh, Y. Zhao, T. Kawakatsu, D. Roccatano, G. Milano, *Phys. Chem. Chem. Phys.* **2014**, 16(11), 5093.
- [11] A. Pizzirusso, A. De Nicola, G. J. Sevink, A. Correa, M. Cascella, T. Kawakatsu, M. Rocco, Y. Zhao, M. Celino, G. Milano, *Phys. Chem. Chem. Phys.* **2017**, 19(44), 29780.
- [12] Y. L. Zhu, Z. Y. Lu, G. Milano, A. C. Shi, Z. Y. Sun, *Phys. Chem. Chem. Phys.* **2016**, 18(14), 9799.
- [13] S. L. Bore, H. B. Kolli, T. Kawakatsu, G. Milano, M. Cascella, *J. Chem. Theory Comput.* **2019**, 15(3), 2033.
- [14] H. B. Kolli, A. De Nicola, S. L. Bore, K. Schäfer, G. Diezemann, J. Gauss, T. Kawakatsu, Z. Y. Lu, Y. L. Zhu, G. Milano, M. Cascella, *J. Chem. Theory Comput.* **2018**, 14(9), 4928.
- [15] S. L. Bore, G. Milano, M. Cascella, *J. Chem. Theory Comput.* **2018**, 14(2), 1120.
- [16] J. T. Padding, W. J. Briels, *J. Chem. Phys.* **2001**, 115(6), 2846.
- [17] J. T. Padding, W. J. Briels, *J. Chem. Phys.* **2002**, 117(2), 925.
- [18] G. PAN, C. W. MANKE, *Int. J. Mod. Phys. B* **2003**, 17(01n02), 231.
- [19] J. D. Schieber, M. Andreev, *Annu. Rev. Chem. Biomol. Eng.* **2014**, 5(1), 367.
- [20] J. D. Schieber, J. Neergaard, S. Gupta, *J. Rheol.* **2003**, 47(1), 213.
- [21] A. E. Likhtman, *Macromolecules* **2005**, 38(14), 6128.
- [22] Y. Masubuchi, J.-I. Takimoto, K. Koyama, G. Ianniruberto, G. Marrucci, F. Greco, *J. Chem. Phys.* **2001**, 115(9), 4387.
- [23] T. Uneyama, Y. Masubuchi, *J. Chem. Phys.* **2012**, 137(15), 154902.
- [24] Y. Masubuchi, *Annu. Rev. Chem. Biomol. Eng.* **2014**, 5(1), 11.
- [25] Y. Masubuchi, *Macromolecules* **2018**, 51(24), 10184.
- [26] Y. Masubuchi, T. Uneyama, *Soft Matter* **2018**, 14(29), 5986.
- [27] V. C. Chappa, D. C. Morse, A. Zippelius, M. Müller, *Phys. Rev. Lett.* **2012**, 109, 148302.
- [28] M. Langeloth, Y. Masubuchi, M. C. Böhm, F. Müller-Plathe, *J. Chem. Phys.* **2013**, 138(10), 104907.
- [29] M. Langeloth, Y. Masubuchi, M. C. Böhm, F. Müller-Plathe, *J. Chem. Phys.* **2014**, 141(19), 194904.
- [30] A. Ramírez-Hernández, B. L. Peters, L. Schneider, M. Andreev, J. D. Schieber, M. Müller, J. J. De Pablo, *J. Chem. Phys.* **2017**, 146(1), 014903.
- [31] G. G. Vogiatzis, G. Megariotis, D. N. Theodorou, *Macromolecules* **2017**, 50(7), 3004.
- [32] Y. Masubuchi, M. Langeloth, M. C. Böhm, T. Inoue, F. Müller-Plathe, *Macromolecules* **2016**, 49(23), 9186.
- [33] M. Kröger, *Comput. Phys. Commun.* **2005**, 168(3), 209.
- [34] S. Shanbhag, M. Kröger, *Macromolecules* **2007**, 40(8), 2897.
- [35] R. S. Hoy, K. Foteinopoulou, M. Kröger, *Phys. Rev. E* **2009**, 80, 031803.
- [36] D. J. Read, K. Jagannathan, A. E. Likhtman, *Macromolecules* **2008**, 41(18), 6843.
- [37] J. Cao, Z. Wang, A. E. Likhtman, *Polymer* **2019**, 11, 496.
- [38] W. C. Swope, H. C. Andersen, P. H. Berens, K. R. Wilson, *J. Chem. Phys.* **1982**, 76(1), 637.
- [39] S. Nosé, *J. Chem. Phys.* **1984**, 81(1), 511.
- [40] S. L. Mayo, B. D. Olafson, W. A. Goddard, *J. Phys. Chem.* **1990**, 94(26), 8897.
- [41] J. Ramos, J. Vega, J. Martínez-Salazar, *Eur. Polym. J.* **2018**, 99, 298.
- [42] V. A. Harmandaris, V. G. Mavrantzas, D. N. Theodorou, M. Kröger, J. Ramírez, H. C. Ottinger, D. Vlassopoulos, *Macromolecules* **2003**, 36(4), 1376.
- [43] K. Foteinopoulou, N. C. Karayiannis, V. G. Mavrantzas, M. Kröger, *Macromolecules* **2006**, 39(12), 4207.
- [44] J. Ramos, J. F. Vega, D. N. Theodorou, J. Martínez-Salazar, *Macromolecules* **2008**, 41(8), 2959.
- [45] A. P. Sgouros, G. Megariotis, D. N. Theodorou, *Macromolecules* **2017**, 50(11), 4524.
- [46] D. Hossain, M. A. Tschopp, D. K. Ward, J. L. Bouvard, P. Wang, M. F. Horstemeyer, *Polymer* **2010**, 51(25), 6071.
- [47] Y. Zhao, A. De Nicola, T. Kawakatsu, G. Milano, *J. Comput. Chem.* **2012**, 33(8), 868.
- [48] A. De Nicola, T. Kawakatsu, F. Müller-Plathe, G. Milano, *Eur Phys J: Special Topics* **2016**, 225(8–9), 1817.
- [49] J. Baschnagel, K. Qin, W. Paul, K. Binder, *Macromolecules* **1992**, 25(12), 3117.
- [50] S. Neyertz, D. Brown, *J. Chem. Phys.* **2001**, 115(2), 708.
- [51] A. E. Likhtman, M. Pomurugan, *Macromolecules* **2014**, 47(4), 1470.
- [52] Y. L. Zhu, H. Liu, Z. W. Li, H. J. Qian, G. Milano, Z. Y. Lu, *J. Comput. Chem.* **2013**, 34(25), 2197.
- [53] J. Schelten, D. Ballard, G. Wignall, G. Longman, W. Schmatz, *Polymer* **1976**, 17(9), 751.
- [54] M. Doi, S. Edwards, *The Theory of Polymer Dynamics*, Oxford University Press, New York, NY **1986**.
- [55] R. S. Graham, A. E. Likhtman, T. C. B. McLeish, S. T. Milner, *J. Rheol.* **2003**, 47(5), 1171.
- [56] R. Everaers, S. K. Sukumaran, G. S. Grest, *Science* **2010**, 823(2004), 823.
- [57] C. Tzoumanekas, D. N. Theodorou, *Macromolecules* **2006**, 39(13), 4592.
- [58] J. Qin, S. T. Milner, *Soft Matter* **2011**, 7(22), 10676.
- [59] J. F. Vega, S. Rastogi, G. W. M. Peters, H. E. H. Meijer, *J. Rheol.* **2004**, 48(3), 663.
- [60] E. van Ruymbek, D. Vlassopoulos, M. Kapnistos, C. Liu, C. Bailly, *Macromolecules* **2010**, 43(1), 525.
- [61] C.-Y. Liu, A. F. Halasa, R. Keunings, C. Bailly, *Macromolecules* **2006**, 39(21), 7415.
- [62] T. Kreer, J. Baschnagel, M. Müller, K. Binder, *Macromolecules* **2001**, 34(4), 1105.
- [63] K. Kremer, G. S. Grest, *J. Chem. Phys.* **1990**, 92(8), 5057.
- [64] M. Monkenbusch, A. Wischnewski, L. Willner, D. Richter, *Phys. B* **2004**, 350(1), 214.
- [65] J. Ramos, J. F. Vega, J. Martínez-Salazar, *Soft Matter* **2012**, 8(23), 6256.
- [66] H. P. Hsu, K. Kremer, *J. Chem. Phys.* **2016**, 144(15), 154907.
- [67] Z. Wang, A. E. Likhtman, R. G. Larson, *Macromolecules* **2012**, 45(8), 3557.
- [68] U. Ebert, L. Schäfer, A. Baumgärtner, *J. Stat. Phys.* **1998**, 90(5–6), 1325.
- [69] K. Hur, C. Jeong, R. G. Winkler, N. Lacevic, R. H. Gee, D. Y. Yoon, *Macromolecules* **2011**, 44(7), 2311.

- [70] K. Z. Takahashi, R. Nishimura, K. Yasuoka, Y. Masubuchi, *Polymer* **2017**, *9*(1), 1.
- [71] A. P. Sgouros, A. T. Lakkas, G. Megariotis, D. N. Theodorou, *Macromolecules* **2018**, *51*(23), 9798.
- [72] M. G. Brereton, *Macromolecules* **1990**, *23*(4), 1119.
- [73] F. Vaca Chávez, K. Saalwächter, *Phys. Rev. Lett.* **2010**, *104*, 198305.
- [74] F. Vaca Chávez, K. Saalwächter, *Macromolecules* **2011**, *44*(6), 1549.
- [75] K. Adachi, T. Kotaka, *Macromolecules* **1984**, *17*(1), 120.
- [76] K. Adachi, T. Kotaka, *Macromolecules* **1985**, *18*(3), 466.
- [77] Y. Zhang, M. Zuo, Y. Song, X. Yan, Q. Zheng, *Comp. Sci. Technol.* **2015**, *106*, 39.
- [78] E. Pilyugina, M. Andreev, J. D. Schieber, *Macromolecules* **2012**, *45* (14), 5728.
- [79] J. P. Montfort, G. Marin, P. Monge, *Macromolecules* **1984**, *17*(8), 1551.
- [80] J. L. Viovy, M. Rubinstein, R. H. Colby, *Macromolecules* **1991**, *24*(12), 3587.
- [81] S. T. Milner, T. C. B. McLeish, A. E. Likhtman, *J. Rheol.* **2002**, *45* (2), 539.
- [82] M. E. Shivokhin, D. J. Read, D. Kouloumasis, R. Kocen, F. Zhuge, C. Bailly, N. Hadjichristidis, A. E. Likhtman, *Macromolecules* **2017**, *50* (11), 4501.
- [83] V. A. Harmandaris, V. G. Mavrantzas, D. N. Theodorou, *Macromolecules* **1998**, *31*(22), 7934.
- [84] T. Glomann, G. J. Schneider, A. R. Brás, W. Pyckhout-Hintzen, A. Wischniewski, R. Zorn, J. Allgaier, D. Richter, *Macromolecules* **2011**, *44*(18), 7430.
- [85] Y. Matsumiya, K. Kumazawa, M. Nagao, O. Urakawa, H. Watanabe, *Macromolecules* **2013**, *46*(15), 6067.
- [86] S. K. Sukumaran, A. E. Likhtman, *Macromolecules* **2009**, *42*(12), 4300.
- [87] P. G. De Gennes, *J. Chem. Phys.* **1971**, *55*(2), 572.
- [88] A. E. Likhtman, M. S. Talib, B. Vorselaars, J. Ramirez, *Macromolecules* **2013**, *46*(3), 1187.
- [89] H. J. Qian, C. C. Liew, F. Müller-Plathe, *Phys. Chem. Chem. Phys.* **2009**, *11*, 1962.
- [90] J. Schneider, L. D. Süß, F. Müller-Plathe, *J. Chem. Eng. Data* **2020**, *65* (3), 1264.
- [91] M. Murat, G. S. Grest, K. Kremer, *Macromolecules* **1999**, *32*(3), 595.
- [92] K. C. Daoulas, M. Müller, J. J. de Pablo, P. F. Nealey, G. D. Smith, *Soft Matter* **2006**, *2*, 573.
- [93] M. Müller, *J. Stat. Phys.* **2011**, *145*(4), 967.
- [94] I. G. Mathioudakis, G. G. Vogiatzis, C. Tzoumanekas, D. N. Theodorou, *IEEE Trans. Nanotechnol.* **2016**, *15*(3), 416.
- [95] S. K. Kumar, V. Ganesan, R. A. Riggleman, *J. Chem. Phys.* **2017**, *147* (2), 020901.

SUPPORTING INFORMATION

Additional supporting information may be found online in the Supporting Information section at the end of this article.

How to cite this article: Wu Z, Kalogirou A, De Nicola A, Milano G, Müller-Plathe F. Atomistic hybrid particle-field molecular dynamics combined with slip-springs: Restoring entangled dynamics to simulations of polymer melts. *J Comput Chem.* 2021;42:6–18. <https://doi.org/10.1002/jcc.26428>